Springer

Available online at https://link.springer.com/journal/42241
http://www.jhydrodynamics.com
Journal of Hydrodynamics, 2022, 34(3): 422-433
https://doi.org/10.1007/s42241-022-0039-y

Assessment of ship maneuvering simulation with different propeller models

Ganbo Deng*, Patrick Queutey, Jeroen Wackers, Michel Visonneau, Emmanuel Guilmineau, Alban Leroyer
LHEEA Lab, Ecole Centrale de Nantes, Nantes, France

(Received March 31, 2022, Revised April 6, 2022, Accepted April 12, 2022, Published online June 24, 2022)

Abstract: This paper is devoted to the assessment of ship maneuvering simulation using different propeller models with the focus on a simplified propeller model that represents the action of the propeller by body force and uses propeller performance curve to determine propeller loading during ship maneuvering. Simulations are also performed with an actual propeller approach with which the propeller rotation is simulated directly with the Reynolds averaged Navier-Stokes equation (RANSE) solver. Both time accurate simulations using sliding grid and rotating frame approximations have been performed for comparison. The zigzag and turning circle maneuvers in calm water have been simulated for two different ship models, namely the ONR tumblehome (ONRT) test case and the KRISO (Korea Research Institute of Ship and Ocean) Container Ship (KCS) test case. Predicted ship motion is compared with measurement data to assess the accuracy of the numerical prediction using RANSE computations with different propeller models.

Key words: Ship zigzag and turning circle motion, simplified propeller model with body force, actual propeller approach

Introduction

Computational fluid dynamics (CFD) can be considered as a mature tool now for steady state ship hydrodynamic applications such as resistance in calm water. Accurate enough predictions can be obtained with reasonable resources even for fully appended hulls, both for model and full scale in a routine design procedure. Self-propulsion computation can also be performed easily with the same cost if a simplified propeller model based on a body force is used. More accurate predictions can be obtained by simulating directly the rotating propeller with sliding or overset grids. For an unsteady application without propeller, such as sea-keeping and planar motion mechanism (PMM) maneuvering motion, simulation can still be performed with affordable computational resources, typically a few days wall clock time with 100 to 200 cores. The situation is different for unsteady flow simulation including a rotating propeller such as zigzag and turning circle maneuvering motion. The most accurate approach for such a configuration is to simulate the rotating propeller directly with a Reynolds averaged Navier-Stokes equation (RANSE) solver. It is usually called discrete propeller approach or actual propeller approach. Since time accurate simulation is required for such simulation and the time step needed to resolve the rotating propeller is very small, such a computation is often very expensive. One month wall clock time or even more is needed using 100 to 200 cores. To reduce the central processing unit (CPU) cost, a propeller model based on body force needs to be used. This will add an additional source of error due to the propeller model. In addition to the above mentioned difficulties related to the propeller, the accurate prediction of ship maneuvering motion is more difficult due to the flow separation around the rudder with high deflection angle and the formation of longitudinal vortex due to drift angle. Nowadays, it is not possible to draw a conclusion based on the published results concerning the predictive capability of CFD simulations for such application. The main objective of the present study is to perform CFD simulation for ship maneuvering application with and without propeller model and compare the result with the measurement data so that different sources of error can be identified.

Our experiences from various validation and verification exercises show that a reliable numerical uncertainty estimation in the case of 3-D unsteady flow as considered here is nearly impossible due to high iterative error as well as time discretization error. Due to high computational cost, no attempt is made to assess space and time discretization error. Instead, the time step as well as the grid density for the original grid (suited for the implemented adaptive grid refinement) in various domains (hull, propellers,

Biography: Ganbo Deng, Male, Ph. D.
Corresponding author: Ganbo Deng,
E-mail: ganbo.deng@ec-nantes.fr

rudders, etc.) are chosen according to our experience in numerical settings for resistance tests and open water simulations in workshops and collaborative studies[1-4].

1. Numerical approach

The flow solver ISIS-CFD, available as a part of the FINE™/Marine computing suite distributed by Cadence Design Systems, is an incompressible unsteady Reynolds-averaged Navier-Stokes (URANS) method mainly devoted to marine hydrodynamics. The method features several sophisticated turbulence models: apart from the classical two-equation k-ω models, anisotropic two-equation explicit algebraic Reynolds stress model (EARSM), as well as Reynolds stress transport models. Hybrid RANS-large eddy simulation (LES) turbulence models based on variants of detached eddy simulation closures (detached eddy simulation (DES)-SST (shear stress transport), delayed DES (DDES)-SST, improved DDES (IDDES)) are also implemented.

The solver is based on the finite volume method to build the spatial discretization of the transport equations. The unstructured discretization is face-based. While all unknown state variables are cell-centered, the systems of equations used in the implicit time stepping procedure are constructed face by face. Fluxes are computed in a loop over the faces and the contribution of each face is then added to the two cells next to the face. Therefore, the grids can be completely unstructured, cells with an arbitrary number of arbitrarily-shaped faces are accepted.

Pressure-velocity coupling is enforced through a Rhie and Chow SIMPLE type method: At each time step, the velocity updates come from the momentum equations and the pressure is given by the mass conservation law, transformed into a pressure equation. In the case of turbulent flows, transport equations for the variables in the turbulence model are added to the discretization. Free-surface flow is simulated with a multi-phase flow approach: The water surface is captured with a conservation equation for the volume fraction of water, discretized with specific compressive discretization schemes[5-6]. Time-integration of Newton's law to solve the 6DOF for ship motion is described in Ref. [7].

To enable relative motions of appendages, propellers or bodies, sliding and/or overlapping grid approaches have been implemented. Propellers can be modeled using actuator disk theory, by coupling with boundary element codes or any other simplified propeller model. It can also be handled by direct discretization of the real propeller through e.g., the rotating frame method or sliding interface approaches[8-9]. Finally, an anisotropic adaptive grid refinement (AGR) procedure has been developed which is controlled by various flow-related criteria. It is also used to improve the accuracy of overset interpolations as it automatically smooth out the cell sizes distribution across overset interfaces between domain[10-11].

Parallelization is based on domain decomposition. The grid is divided into different partitions, which contain the cells. The interface faces on the boundaries between the partitions are shared between the partitions; information on these faces is exchanged with the message passing interface (MPI) protocol. This method works with the sliding/overlapping grid approaches and the different sub-domains can be distributed arbitrarily over the processors without any loss of generality. Moreover, the AGR procedure is fully parallelized with a dynamic load balancing working transparently with or without sliding or overlapping grids.

2. Simplified propeller model

When a body force approach is used to simulate the propeller, the propeller model is critical for the accuracy of the simulation. The simplified propeller model used in the present study is inspired by the coupling procedure between RANSE and boundary element method (BEM) solvers for propeller modelling. The RANSE-BEM coupling procedure is implemented in the following way. First, the RANSE solver provides the velocity field in front of the propeller as total velocity to the BEM code. The potential code computes the propeller induced velocity at the same position and deduces the effective wake. The effective wake is used as boundary condition in the BEM code to compute the propeller performance and represent the action of the propeller by body forces. Those body forces are then added as source term in the momentum equation for the RANSE simulation. There are two different ways to run the BEM code. The first way is to run a steady computation. In this case, the effective wake is averaged in the circumferential direction, so is the body force. The advantage of such a computation is that the CPU cost is very low, typically a few seconds. But the result is less accurate. To reach a better accuracy, an unsteady computation needs to be performed using the effective wake directly without averaging. Body force is averaged in time only. The key issue in the coupling procedure is how to determine accurately the effective wake in the propeller plane. Since the propeller induced velocity is computed by the BEM code, the body force needs to be represented as accurately as possible. Besides, the coupling plane is located in front of the propeller. To obtain the effective wake in the propeller plane,

additional approximation is needed. We can replace the BEM code by the propeller performance curve to obtain a simple propeller model. This simple propeller model is implemented in a similar way. The RANSE solver computes the mean velocity at the propeller plane. Another RANSE open water computation with body force is performed to obtain the propeller induced velocity. This open water RANSE computation can be performed independently. The propeller induced velocity can then be obtained by interpolation from the results of open water RANSE computation. Subtracting the mean velocity at the propeller plane from the propeller induced velocity will give us the propeller advancing speed. With the propeller advancing speed, we can determine the propeller thrust and torque from the propeller performance curve. Body forces are added in the source term of the momentum equation by using an empirical force distribution. This approach is not as accurate as a BEM code, since the effective wake distribution as well as the direction of the inflow velocity cannot be represented. The advantage of this propeller model is its simplicity. It is only necessary to provide a propeller performance $Kt-Kq$ curve. There is no additional cost in the simulation. Propeller geometry is not needed except for the open water computation to obtain this $Kt-Kq$ curve. In our present study, open water measurement data is used for this input. However, the drawbacks of this propeller model are the following. It responds to the mean axial velocity only. Non-uniform wake distribution as well as oblique inflow angle cannot be taken into account. Moreover, only axial and tangential forces are taken into account. Side force effect is missing. Besides, forces are averaged in the circumferential direction, which may have an impact on the rudder operating behind the propeller.

3. Case setup

3.1 *ONRT ship model*

The ONR tumblehome (ONRT) ship hull model, length $L_{pp} = 3.147$ m, Fig. 1, is appended with a skeg and bilge keels. The model has also twin rudders, shafts and two 4-bladed propellers with shaft brackets. The rudders are of the spade type. The propellers are fixed pitch type with the direction of rotation inward over the top.

It is the 5.2 test case of the SIMMAN workshop initially scheduled for 2019. Main particulars are described in http://www.simman2019.kr/contents/test_case_5.2.php and are not included here again for the sake of brevity. This reference contains also all the recommendations to simulate the 20°/20° starboard (SB) side zigzag maneuver in calm water starting with a first step exercise to evaluate the self-propulsion point at $Fr = 0.2$ (target speed $U = 1.11$ m / s).

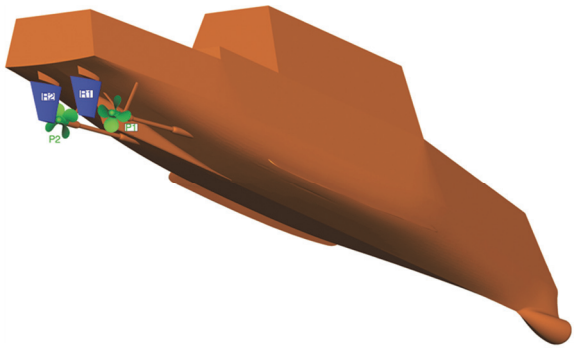

Fig. 1 (Color online) Numerical model of the ONRT

The choice of the mass m, inertia matrix $\mathbf{I}$ and location of the center of gravity is critical to solve the 6DOF for simulations as close as possible to the experimental conditions. Our choice comes first from the prescribed draft 0.112 m. Therefore the closed solid bodies (Fig. 1) gives the numerical mass 73.7582 kg and CG coordinates=(1.625 m, 0 m and 0.044 m) so that the numerical model is in equilibrium at rest (water density 999.19 kg/m³). The reference frame is such that the bow is at $x = 0$ m with x-axis pointing towards AP and $z = 0$ defines the plane of free-surface at rest. Serious doubts were raised after the Tokyo 2015 workshop about the value of kxx coefficient which define Ixx $(m \cdot kxx^2)$. From numerical roll damping in calm water at zero advance speed in the context of NATO/AVT-280 collaborative research project, we retained $kxx = 0.34B$ (ship breadth $B = 0.384$ m) which appears to be a reasonable choice to us (computed roll period 1.61 s) compared with the original $0.44B$ (computed roll period 1.81 s), close to the $0.344B$ proposed now in case 5.2 of the workshop. For the other coefficients Iyy, Izz (yaw, pitch), we keep the proposed radius $0.246L_{pp}$.

Overset grid is used to handle ship free motion. A small ship domain is free to move with rigid mesh motion inside a background domain. Additional domains are created for the two propellers and for the two rudders. There are six domains to be meshed independently by HEXPRESS™, which results in a unique grid to be partitioned.

While sliding interfaces are considered between the ship and the propeller domains, overset interpolation is preferred between the ship domain and the background, and between the rudder and the ship

domains. AGR is therefore very advantageous to minimize the interpolation errors across these interfaces.

Figures 2, 3 are illustrative of the grid behavior during the zigzag maneuver in a constant $-z$ or $-x$ plane passing through the propeller center. In each domain the grid moves rigidly: Rotating motion around the propeller axis or around the rudder axis.

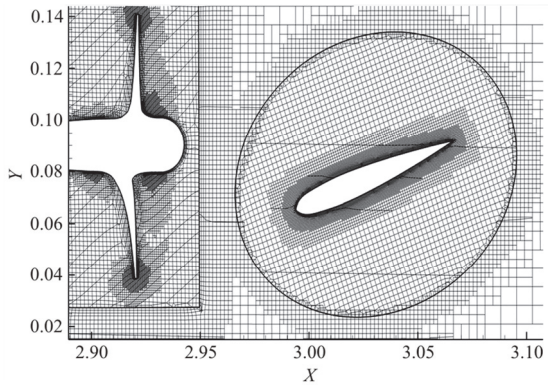

Fig. 2 Adapted grid in horizontal plane and close to propeller and rudder at an arbitrary time instant

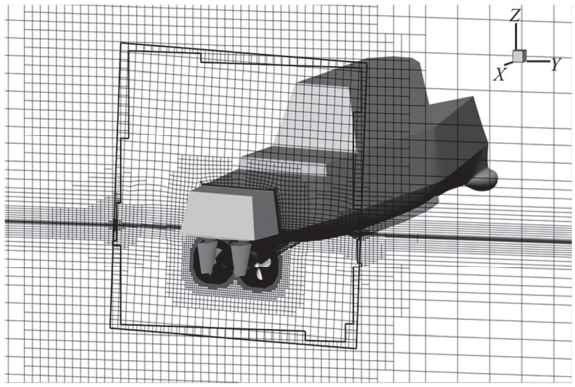

Fig. 3 Adapted grid in longitudinal plane through propeller centers at an arbitrary time instant

As our objective is not to precisely simulate the experimental basin with influence of its walls, the background domain is moving but recovers only the (x, y) translations and the yaw of the ship DOF Inside the background, the ship domain is free to move, still rigidly, according to the roll, pitch and heave motions. Again, AGR is used to ensure the accuracy of the overset interpolations between the ship and the background domain and also to improve the interface capturing (with the help of combined criteria).

The background domain extension is $[-20\text{ m}, 20\text{ m}]\times[-10\text{ m}, 10\text{ m}]\times[-2L_{pp}, 0.5L_{pp}]$ with far-field boundary conditions on its vertical planes and prescribed pressure on top and bottom. Wall-function (target y^+ about 40) is applied on all surfaces of the ship model.

3.2 *KCS ship model*

This is the test case 3.2 of the SIMMAN 2019 workshop. The scale factor of the ship model is 37.89, giving a $L_{pp} = 6.07$ m. The target speed is 2.005 m/s with a Froude number $Fr = 0.26$. Unlike the previous case, a big ship domain is used without having recourse to a background domain. An overset domain is used for the rudder, while a sliding grid domain is used for the propeller for the actual propeller approach. The ship domain extension is $[-19.2\text{ m}, 19.2\text{ m}]\times[-12\text{ m}, 12\text{ m}]\times[-7.79\text{ m}, 3.41\text{ m}]$. The mid ship is located at $x = 0$. For the computation using body force, the ship domain and the rudder domain contain 4.17×10^6, 1.81×10^6 cells respectively, while for the case with actual propeller, there are 4.59×10^6, 1.12×10^6 and 1.12×10^6 cells in the ship domain, rudder domain and the propeller domain, respectively. During the computation, AGR adds about 30% more cells to capture the free surface as well as to ensure cell size continuity near the overset interface. The geometry of the KCS ship model used in the CFD simulation is shown in Fig. 4. The propeller is separated from the hull with a gap so that both the ship and the propeller form a closed body. Hence, the force acting on the hull can be compared directly between different propeller models.

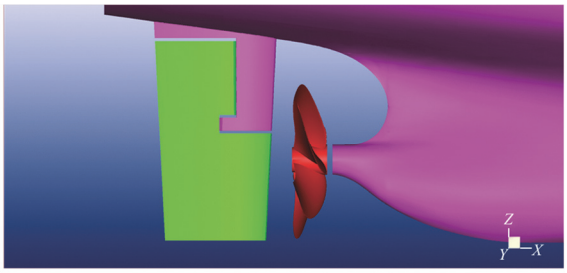

Fig. 4 (Color online) The KCS ship model

4. Numerical setting and models

As stated in the introduction, the main objective of the study is to test if the use of simplified propeller model is a cost-effective alternative to full modeling where the only uncertainty would be the turbulence modeling. To this purpose, we considered three approaches:

(1) Actuator disk (AD) model

It is the body force approach with actuator disk model where the Kt-Kq curves from open water (experimental fluid dynamics (EFD) or CFD) are used to update the thrust and the torque during the simulation when the propeller revolution per second

(rps) is imposed, or to determine the propeller rps in a self-propulsion simulation. The time step is similar to the time step used for resistance in calm water, typically $0.5L_{pp}/U/100$ rounded to 0.01 s.

(2) Rotating frame method (RFM) model

The rotating frame method in ISIS-CFD is used to model a general rigid-body motion (rotation) where the RANS equations are solved in the rotating reference frame but written in terms of absolute or inertial frame quantities. For example, it allows a steady calculation in case of open-water propeller or when the flow is steady in the rotating frame. The time step used is therefore the same as for the AD model, i.e., 0.01 s.

(3) Actual propeller (AP) model

The actual propeller is solved to provide a reference solution. The time step is therefore driven by the rps of the propeller (typically 2° per time step). For the ONRT test case, with a propeller revolution rate about 9 rps, the time step is about 0.0006 s, 17 times smaller than AD or RFM models. For the KCS test case, since the time step used for the computation for the AD model is twice as big (0.02 s), and the propeller rps is higher (about 12 rps), the time step ratio is 46. Then the AP model CPU cost is expected to be approximately 17 times and 46 times more expensive than with simplified propeller models for the ONRT and the KCS test case, respectively.

For the ONRT test case, the propeller is meshed for RFM and AP models. In the computation with body force, the blades in the propeller domain are removed, the domain containing only the shaft. This way simplifies the mesh implementation and only two original grids are used for all the simulations, see Table 1. In both cases, the target vertical size in the original grid around the free-surface at rest is $L_{pp}/500$ (7.5 mm).

Table 1 Original mesh sizes in million cells

Domain	RFM or AP	AD
Background	1 432 364	1 432 364
Ship	4 432 597	4 320 701
1 propeller	1 151 019	725 472
1 rudder	2 263 062	2 263 062
Total	12 693 123	11 729 503

5. Results and discussions

5.1 *ONRT self-propulsion step*

The maneuver is performed at a fixed rps evaluated from a self-propulsion simulation. The rps depends on the model used AD, RFM or AP.

AP and RFM models: to find the revolution rate of the propellers corresponding to the target speed of the ship in calm water $U=1.11\,\mathrm{m/s}$, two simulations are conducted around the 8.97 rps known from EFD, one 15% higher and the second 10% lower. In these simulations in calm water, only heave and pitch motions are solved and rudders are fixed. When the forces for ship resistance and the propeller thrust are established, the towing force for each simulation is deduced by the difference between the ship resistance and the propeller thrust. The self-propulsion point for which the towing force is zero is determined by linear interpolation between the above two operation points. The RFM approach is surprisingly closer to EFD with 8.97 rps than the AP model with 8.73 rps (4.4% error). However, the good RFM prediction could be explained by the fact that the propellers are positioned laterally and do not operate directly in the wake of the ship.

The self-propulsion point with the AD model is found directly by adjusting the body force coupled with the $Kt-Kq$ curves during the simulation and prediction is 8.93 rps (0.5% error).

5.2 *ONRT 20°/20° starboard side zigzag motion*

For each model, simulation is simply restarted from the self-propulsion step releasing this time all 6DOF and rudder motion such that the rudder rate is 35°/s with direct control from the computed yaw according to the zigzag rules, see Fig. 5 for notations.

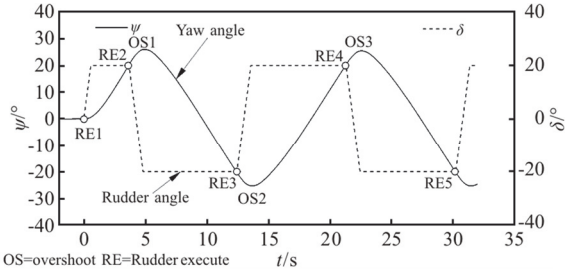

Fig. 5 20°/20° zigzag rules and notations where RE means Rudder Execute, OS for overshoot of the computed ship's yaw ψ, δ is the controlled rudder angle

Due to available CPU resources only the SB zigzag for a total duration of 25 s to 30 s in physical time is considered. Parallel simulations are performed over 168 partitions for RFM and AP models and 160 for AD model. Simulations have been performed in one shot only without trying to optimize the CPU but keeping very conservative criteria to prioritize the quality of resolution (for linear systems and iterative coupling). If AD model is taken as a reference with a total CPU cost of 8×10^3 h (2 days wall clock time) for 2.5×10^3 time steps, RFM cost is nearly the same with about 1.3 time the AD model but, as expected, the AP model cost with 4×10^4 time steps is 16.5 times higher (about 1 month wall clock time).

The time history of the relative increase of the number of cells from the original grid with AP is plotted in Fig. 6 where some significant aspects of the zigzag manoeuver (RE, OS) are indicated. Time 0 is the time of the first RE after a restart from the self-propulsion step. It shows that the most important efforts produced by AGR (by only 15%) are between two consecutive RE actions: From the ship and rudder motions and also from the free-surface changes where the vertical resolution of the anisotropic refinement goes until 1.8 mm (a factor 4 from the original grid). Figure 6 already shows that a periodic state of the zigzag motion seems to be already established after the first OS.

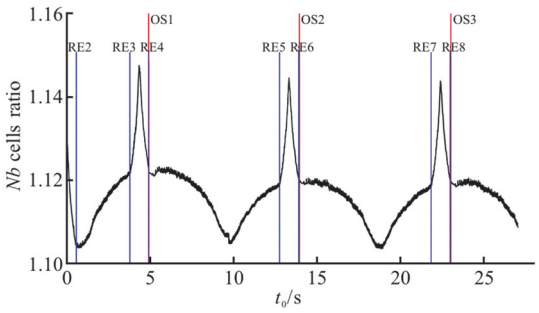

Fig. 6 (Color online) Time history of the increase in cell number with AP model

Results of post-processing of trajectory and time histories of some DOF are compared between different propeller models and also to available EFD measurements[12-13]. EFD data from Refs. [12-13] have been simply digitized and therefore must be taken as such. These EFD data are used as an indication to qualify the propeller models. In all the following figures, the scanned measurements are represented by points and the result of the simulations by curves. The trajectory of the ship in Fig. 7 is the motion of the mid-ship point O $(x(t), y(t), z = 0)$. AP and AD models are in line with EFD with a slight improvement for AP. RFM method leads to an increasingly stretched trajectory along x.

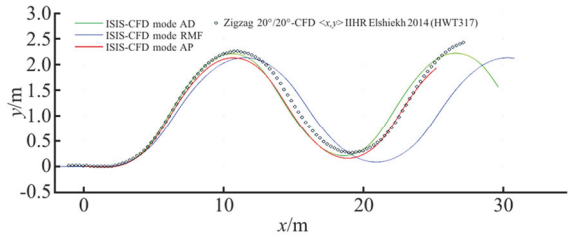

Fig. 7 (Color online) Trajectory of the ship mid-point O in horizontal plane (x, y)

This is consistent with the ship speed history, Fig. 8, as the surge and the sway velocities from RFM are over- and underestimated, respectively. The most negative effect of RFM is too low a sway velocity. The drawback of the RFM approach can be attributed to the fact that the propeller side force is poorly predicted since the propeller blades are frozen in the computation. Based on the time history of the transversal force Fy on a rudder and compared to AP result, Fig. 9, it is clear that the propeller/rudder interactions are not correctly predicted with the RFM approach. On the other hand, although the predicted Fy force on the rudder is quite different between the AP and the AD approaches, the predicted yaw angle as shown in Fig. 10 by the two methods is almost the same. This can be explained by the fact that the side force of the propeller induces an additional side force in the opposite direction both on the hull and on the rudder. Consequently, global yaw moment acting on the hull is almost the same, although the side force acting on the rudder is quite different.

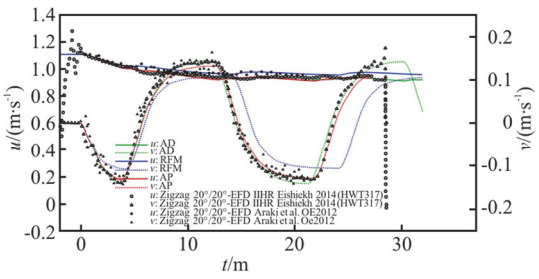

Fig. 8 (Color online) Time history of the ship speed components (surge u, sway v)

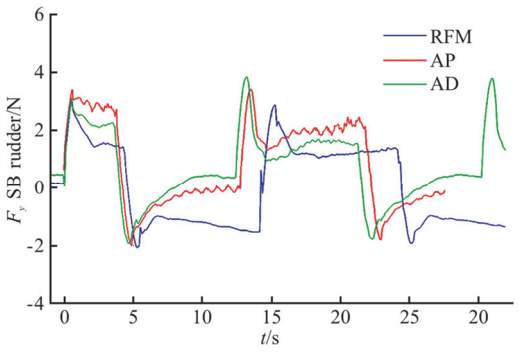

Fig. 9 (Color online) Time history of transversal force Fy on the starboard rudder (in the frame linked to the rudder)

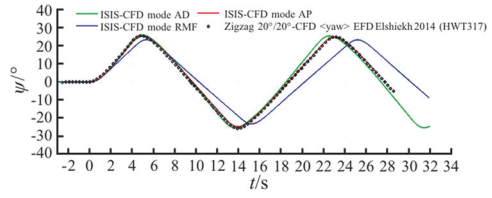

Fig. 10 (Color online) Time history of the yaw angle

The time histories of the yaw and the rudder angles are presented in Figs. 10, 11. The control by RFM is systematically late while AD performs fine although slightly in advance on OS3 (a shorter time period). AP model performs nicely, in agreement with the EFD data.

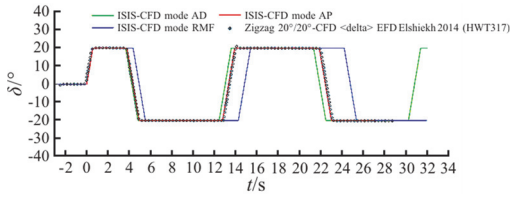

Fig. 11 (Color online) Time history of the rudder angle

The time history of the roll angle is presented the same way in Fig. 12. There is a remarkable agreement between the prediction obtained by the AP model and the digitized EFD from Ref. [13], both in time and amplitude with all the main frequencies captured. Same conclusions hold for AD model with a motion period underestimated and in the opposite for RFM.

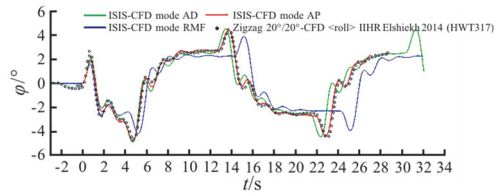

Fig. 12 (Color online) Time history of the rudder angle

This is an indirect verification for the choice of the *kxx* inertia coefficient $0.34B$ (the proposed $0.344B$ would not change significantly the result).

An analysis of the flow details, correlated with motion and force histories, in order to understand the defaults of a propeller model and of physical modeling (turbulence) is extremely difficult to carry out here. As an example, Figs. 13, 14 compare the instantaneous distributions of the axial velocity and the turbulence kinetic energy (TKE) in a vertical plane through the propeller center at a time when the yaw returns to zero between OS1 and OS2 (see Fig. 5). The trace of high velocity region shown in Fig. 13 is the imprint of the drift angle. It can be seen from Fig. 13 that the AP and the AD models give similar prediction, while the result obtained by the RFM approach suggests a lower drift angle. The AD model produces lower TKE levels than the resolved propeller. It is reminded that conventional linear eddy-viscosity type turbulence models fail to predict separated flow with accuracy. Here, if the flow in the propeller/rudder interaction is driven by the pressure with low occurrence of separation (to be confirmed) then it could explain why, although the TKE distributions are different, the AD model is still in line with the AP model.

A better overview of flow details in that region can be accessed from this link with a video for the AP model: https://youtu.be/5RpZexkz9pY.

5.3 *KCS self-propulsion step*

Similar to the ONRT test case, a self-propulsion simulation has been performed first to determine the propeller revolution speed used in the maneuvering simulation. The propeller rps is adjusted to match the model scale self-propulsion point with the target ship speed of 2.006 m/s. The measurement data is $n = 11.41$ rps. The AD approach predicts $n = 11.65$ rps with 2.1% over prediction, while the AP approach gives a higher value $n = 11.94$ rps with 4.7% over prediction. We believe that the over prediction obtained by the AP approach is mainly due to turbulence modelization. At model scale, the flow near the leading edge of the blade is more likely in a transitional regime, while the RANSE model with wall function is employed in the CFD simulation in order to save CPU time. Consequently, the thickness of the turbulence boundary layer in the CFD simulation is higher, resulting in a lower propeller thrust and

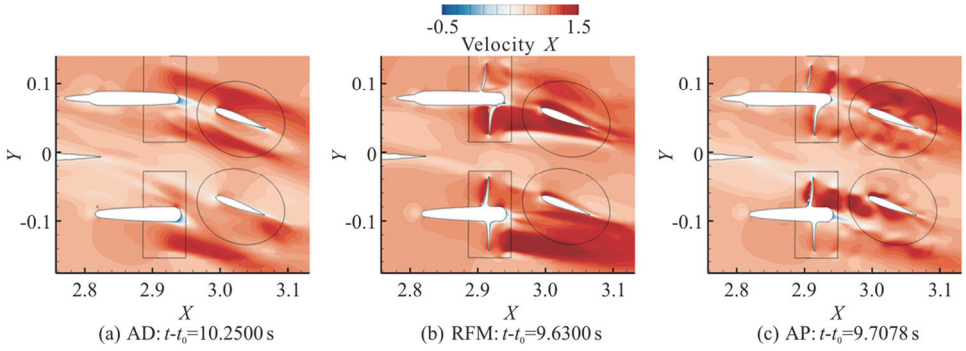

Fig. 13 (Color online) Instantaneous contour distribution of axial velocity in a cut plane

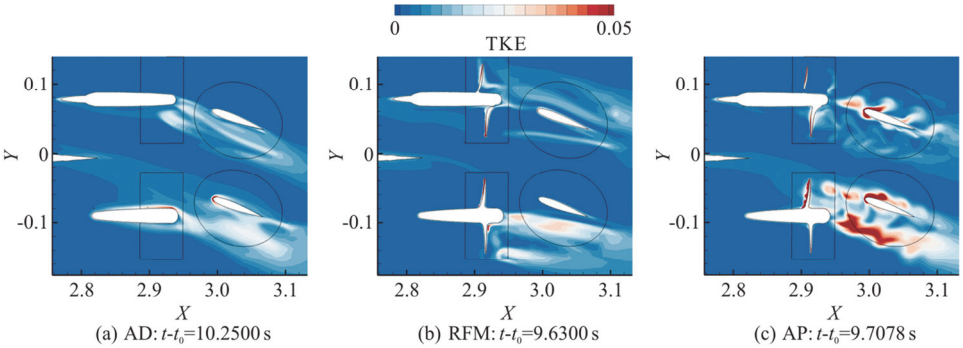

Fig. 14 (Color online) Instantaneous contour distribution of the TKE in a cut plane

higher propeller torque. A higher propeller revolution rate is therefore needed to achieve the self-propulsion equilibrium.

5.4 *KCS 20°/20° starboard side zigzag motion*

The zigzag motion simulation for the KCS test case is performed with a setup similar to the ONRT test case. Since the prediction with the RFM approach is very poor, only the AD model and the AP model are compared for this test case. The predicted yaw angle is compared with the measurement data obtained by MARIN in Fig. 15. Compared to the previous test case, the CFD predictions are less satisfactory, especially with the AD model. Such behaviors can be attributed to the type of rudder. A semi-spade type of rudder is used in the KCS test case. The gaps between the mobile part and the fixed part of the rudder makes the flow separate more easily from the rudder even at small rudder deflection angle. As separated flows are usually not well predicted with RANSE turbulence model, more discrepancies are observed as expected.

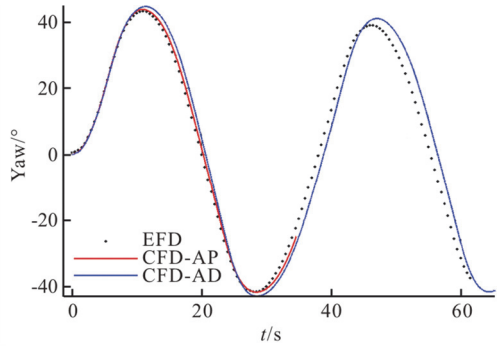

Fig. 15 (Color online) Time history of yaw angle for the KCS zigzag 20°/20° motion

The better prediction with the AP model can be attributed to its capability to take into account the effect of propeller side force. Before the second rudder execution, the propeller side force is acting in the opposite direction to the rudder side force as shown in Fig. 16. Moreover, it induces an additional side force in the opposite direction both on the rudder and on the hull. Consequently, both propeller models give similar prediction for the yaw angle. Shortly after the second rudder execution starting from $t = 6$ s, the direction of the propeller side force coincides with that of the rudder side force up to about $t = 12$ s when the drift angle changes the sign. During this period, propeller side force makes the ship turn faster compared to the case with AD model, resulting in a better prediction of the first overshoot angle. Later on, it is more difficult to analyse the effect of propeller side force. For instance, when the ship is at its maximum drift angle near $t = 20$ s, the difference on the side force predicted by two different propeller models on the hull is more important than the rudder side force. Moreover, propeller side force does not induce an additional side force on the rudder in the opposite direction as observed previously. There must be an interaction between the propeller side force and the flow separation around the rudder as well as the interaction with the longitudinal vortex developed along the hull.

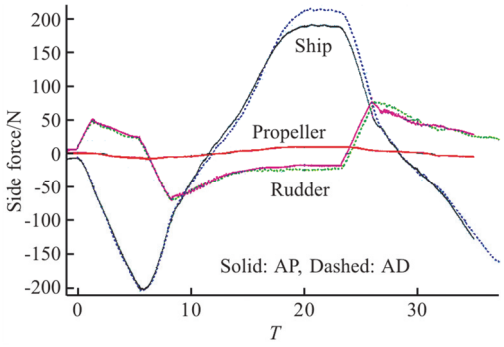

Fig. 16 (Color online) Time history of side force for the KCS zigzag 20°/20° motion

The predicted roll angle is displayed in Fig. 17. Both propeller models are capable to provide a good prediction compared with measurement data with a

better agreement observed with the AP model. However, it is difficult to extract more useful information from this comparison.

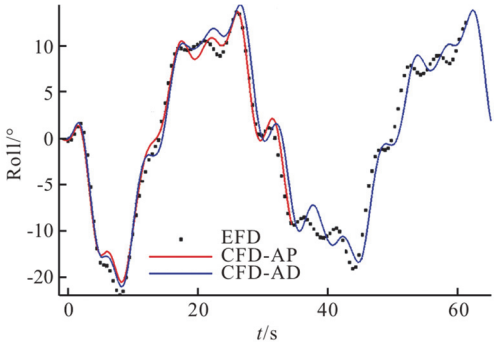

Fig. 17 (Color online) Time history of the roll angle for the KCS zigzag 20°/20° motion

The predicted surge velocity is compared in Fig. 18. It is observed that the AP model over predicts the surge velocity. By looking at the predicted surge force shown in Fig. 19, we can conclude that the over prediction of the surge velocity by the AP model is mainly due to a higher predicted propeller thrust at the beginning the zigzag motion. However, we do not think that this higher predicted propeller thrust is due to a poor prediction of the AP model, compared with the AD model. The reason of the over predicted surge velocity by the AP model is more likely due to the under-prediction of rudder resistance. The difference between the two propeller models on the surge force is also observed on the hull near $t = 20$ s when the drift angle is maximum. This observation suggests that there must be an interaction between the propeller and the longitudinal vortex developed along the hull, which cannot be captured by the body force model. Further investigation is needed. The drift angle is compared in Fig. 20. The measurement data is shifted down due to the initial condition. There is an initial yaw angle in the measurement before the zigzag motion starts which is not simulated in the computation.

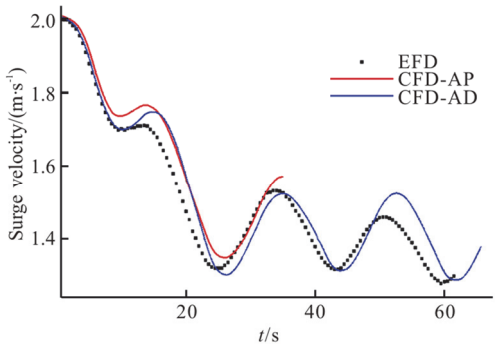

Fig. 18 (Color online) Time history of surge velocity for the KCS zigzag 20°/20° motion

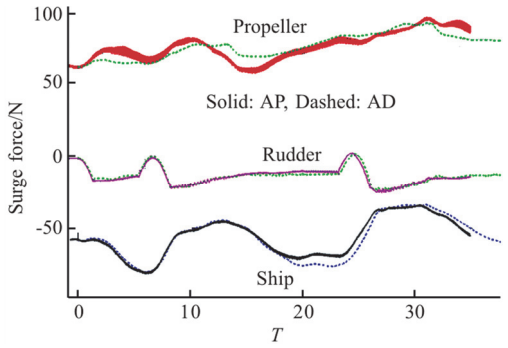

Fig. 19 (Color online) Time history of surge forces for the KCS zigzag 20°/20° motion

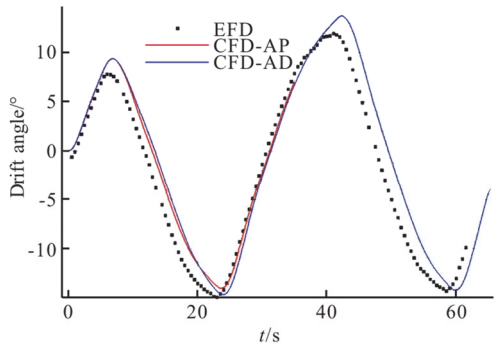

Fig. 20 (Color online) Time history of drift angle for the KCS zigzag 20°/20° motion

5.5 *KCS 35° starboard side turning circle motion*

The initial condition of the turning circle motion is the same as the zigzag motion. Starting from the established self-propulsion solution, the rudder angle changes from 0° to 35° within 2.44755 seconds with a rudder rate of 14.3°/s. All 6DOF of the ship are free. After a transient period, the flow reaches a steady state where all quantities in the ship coordinate system remain almost constant. The trajectory of the TC35 (turning circle 35°) motion is displayed in Fig. 21. The predictions given by both propeller models are similar. The predicted radius for the steady gyration motion by the AP model is almost the same as the measurement data, while the AD model under predicts it by less than 2%. Both models suffer a common drawback compared with measurement result. The predicted yaw angle is noticeably smaller than the measurement result. Since the RANSE turbulence model under predicts the propeller side force at large rudder deflection angle as shown in a previous study[14], turbulence modelization error is expected to be the main cause of this deficiency. Another possible reason is the experimental condition. During this period, the ship model might be very close to the wall which might force the ship model to turn faster. Not shown

in this paper, the port side turning circle simulation of the same case provides a much better agreement during this period. Numerical discretization error may also have a contribution since the mesh used in the present simulation is not very fine, and the AGR is used to capture the free surface and to ensure cell size continuity for the overset interface only. Further investigations are needed to quantify this error.

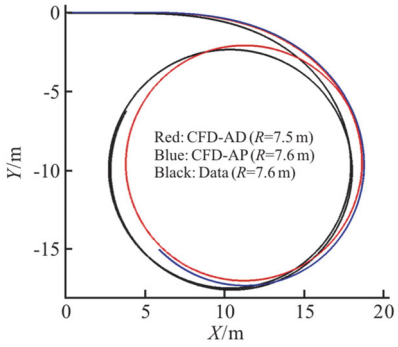

Fig. 21 (Color online) Trajectory of the KCS TC35 motion

The predicted surge velocity is compared in Fig. 22. The prediction obtained by the AD model agrees well with the measurement data, while the AP model over predicts the surge velocity. In order to better understand the reason, the predicted surge force on the ship, on the rudder and on the propeller are compared in Fig. 23. The AP model predicts a higher propeller thrust. It induces a higher ship resistance as expected. The force acting on the hull and the propeller combined is higher during the transient period with the AP model, but they are almost identical at steady state. On the other hand, rudder resistance decreases rather than increases with the AP model. We believe that it is this under-estimation of rudder resistance due to turbulence modelization error that is responsible for the over estimation of surge velocity observed with the AP model.

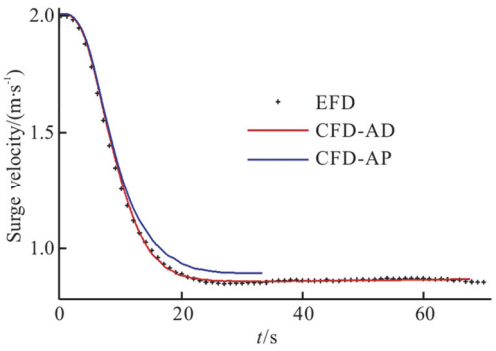

Fig. 22 (Color online) Time history of surge velocity for the KCS TC35 motion

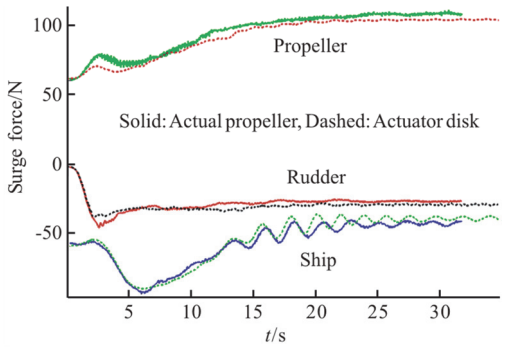

Fig. 23 (Color online) Time history of surge force for the KCS TC35 motion

The drift angle is compared in Fig. 24. CFD predictions agree well with the measurement during the transient period, but over predict the drift angle for the steady state. Since the relative rudder angle in the steady state is small, which makes the CFD prediction for the flow around the rudder more accurate, we believe that this discrepancy is due to the turbulence modelization error and spatial discretization error in the prediction of longitudinal vortex formed at the bow, which is expected to be higher at high drift angle.

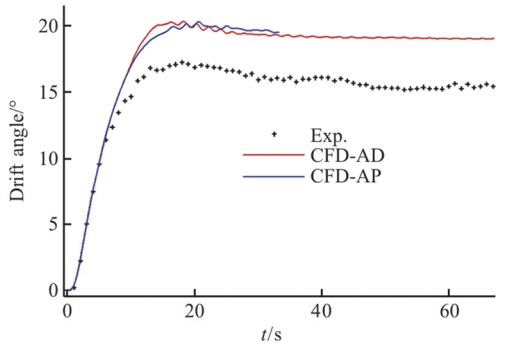

Fig. 24 (Color online) Time history of drift angle for the KCS TC35 motion

Side forces acting on the hull, rudder and the propeller are compared in Fig. 25. It can be observed that the effect of propeller side force is limited for this test case. For completeness, CFD prediction for roll angle and yaw rate are compared in Figs. 26, 27 respectively. It is however difficult to extract useful information from these comparisons.

6. Conclusion

The zigzag and turning circle maneuvers have been computed for the ONRT and the KCS test cases with the help of the ISIS-CFD flow solver. The numerical setting for the study is considerably simplified by the use of the overset technology combined

with anisotropic adaptive mesh refinement and de-refinement. Three propeller models have been used and compared, from body force (AD) to a frozen-rotor like method (RFM) and with the actual propeller as a reference. The main conclusion is that the implemented AD model is cost effective, about 20 to 40 times faster compared with the propeller resolved simulations with a reasonable agreement between the two concerning the trajectory and the motions. A more accurate prediction is reached for the ONRT test case equipped with a spade type rudder. On the other hand, the RFM approach is unsuitable for such kind of simulation due to the poor prediction of propeller side force. While the propeller side force is correctly predicted by using the AP model, its effect has been found limited on the predicted motion, although the difference in the predicted forces and the moments on the rudder and the hull are noticeable. However, taking into account the propeller side force always results in an improved prediction. In addition to propeller model, turbulence modelization error for the prediction of the separated flow around the rudder at high rudder angle, especially for the semi-spade type propeller, as well as for the prediction of longitudinal vortex at high drift angle is also responsible for the discrepancies observed between the CFD simulation and the measurement.

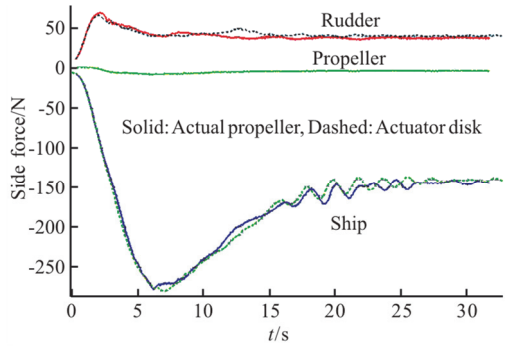

Fig. 25 (Color online) Time history of side force for the KCS TC35 motion

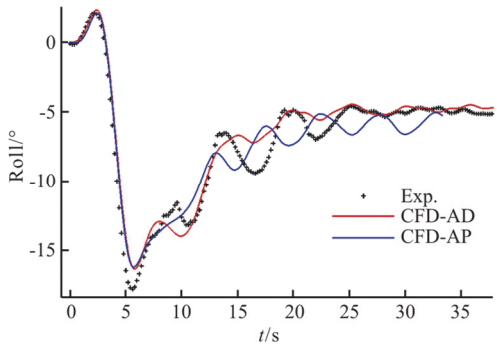

Fig. 26 (Color online) Time history of roll angle for the KCS TC35 motion

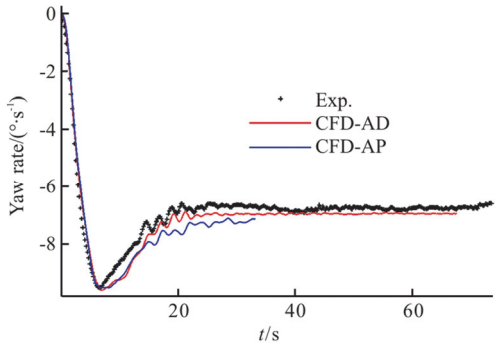

Fig. 27 (Color online) Time history of yaw rate for the KCS TC35 motion

Acknowledgements

This work was made possible thanks to granted access to the HPC resources of CINES and IDRIS computing centers under the allocation A0072A01308 made by Grand Equipement National de Calcul Intensif (GENCI).

References

[1] Guilmineau E., Deng G., Queutey P. et al. URANS simulations of planar motion mechanism for two hulls [C]. *Workshop on Verification and Validation of Ship Manoeuvering Simulation Methods (SIMMAN-2014)*, Lyngby, Denmark, 2014.

[2] Deng G., Leroyer A., Guilmineau E. et al. Verification and validation of resistance and propulsion computation [C]. *Proceedings of Tokyo 2015-A Workshop on Numerical Ship Hydrodynamics*, Tokyo, Japan, 2015.

[3] Guilmineau E., Deng G., Leroyer A. et al. Numerical simulations for the wake prediction of a marine propeller in straight-ahead flow and oblique flow [J]. *Journal of Fluid Engineering*, 2018, 140(2): 021111.

[4] Bhushan S., Yoon H., Stern F. et al. Assessment of CFD for surface combatant 5415 at straight ahead and static drift $\beta = 20°$ [J]. *Journal of Fluids Engineering*, 2019, 141(5): 051101.

[5] Queutey P., Visonneau M. An interface capturing method for free-surface hydrodynamic flows [J]. *Computers and Fluids*, 2007, 36(9): 1482-1510,.

[6] Wackers J., Koren B., Raven H. C. et al. Free-surface viscous flow solution methods for ship hydrodynamics [J]. *Archives of Computational Methods in Engineering*, 2011, 18(1): 1-41.

[7] Hay A., Leroyer A., Visonneau M. H-adaptative Navier-Stokes simulations of free-surface flows around moving bodies [J]. *Journal of Marine Science and Technology*, 2006, 11(1): 1-18.

[8] Queutey P., Wackers J., Leroyer A. Dynamic behaviour of the loads of podded propellers in waves: experimental and numerical simulations [C]. *The 33nd International Conference on Ocean, Offshore and Arctic Engineering*, San Francisco, USA, 2014.

[9] Gao X., Deng G. To evaluate the influence of DOF on maneuvering predictions by direct CFD zig simulations

[C]. *VIII International Conference on Computational Methods in Marine Engineering*, Göteborg, Sweden, 2019.
[10] Wackers J., Deng G. B., Leroyer A. et al. Adaptive grid refinement for hydrodynamic flows [J]. *Computers and Fluids*, 2012, 55: 85-100.
[11] Wackers J., Deng G., Guilmineau E. et al. Combined refinement criteria for anisotropic grid refinement in free-surface flow simulation [J]. *Computers and Fluids*, 2014, 92: 209-222.
[12] Araki M., Sadat-Hosseini H., Sanada Y. et al. Estimating maneuvering coefficients using system identification methods with experimental, system-based, and CFD free-running trial data [J]. *Ocean Engineering*, 2012, 51: 64-84.
[13] Elshiekh H. A. Maneuvering characteristics in calm water and regular waves for ONR Tumblehome [D]. Master Thesis, Iowa, USA: The University of Iowa, 2014.
[14] Deng G., Leroyer A., Guilmineau E. et al. Effect of turbulence modelization in hull-rudder interaction simulation [C]. *Proceedings of the 30th National Conference on Hydrodynamics and15th National Congress on Hydrodynamics*, Hefei, China, 2019.